

Adsorption and reaction of sulfur dioxide with Cu(110) and Cu (110)-p(2×1)- O

Ali R. Alemozafar, Xing-Cai Guo, and Robert J. Madix

Citation: *The Journal of Chemical Physics* **116**, 4698 (2002); doi: 10.1063/1.1450545

View online: <http://dx.doi.org/10.1063/1.1450545>

View Table of Contents: <http://scitation.aip.org/content/aip/journal/jcp/116/11?ver=pdfcov>

Published by the [AIP Publishing](#)

Articles you may be interested in

Oxygen adsorption-induced nanostructures and island formation on Cu{100}: Bridging the gap between the formation of surface confined oxygen chemisorption layer and oxide formation

J. Chem. Phys. **129**, 124703 (2008); 10.1063/1.2980347

Adsorption of α -pyridone on Cu(110)

J. Chem. Phys. **116**, 8988 (2002); 10.1063/1.1471244

Adsorption, decomposition, and stabilization of 1,2-dibromoethane on Cu(111)

J. Vac. Sci. Technol. A **19**, 1474 (2001); 10.1116/1.1376702

Adsorption of hydrogen on clean and potassium modified low index copper surfaces: Cu(100) and Cu(110)

J. Vac. Sci. Technol. A **19**, 1988 (2001); 10.1116/1.1359552

Elevated temperature scanning tunneling microscopy study of formic acid adsorption and reaction on oxygen (2×1) covered Cu(110)

J. Chem. Phys. **108**, 6916 (1998); 10.1063/1.476106



Adsorption and reaction of sulfur dioxide with Cu(110) and Cu(110)- $p(2\times 1)$ -O

Ali R. Alemozafar, Xing-Cai Guo, and Robert J. Madix^{a)}

Department of Chemical Engineering, Stanford University, Stanford, California 94305-5025

(Received 24 September 2001; accepted 20 December 2001)

On Cu(110)- $p(2\times 1)$ -O at 300 K $\text{SO}_2(g)$ reacts stoichiometrically with O(a) to form a surface covered with both $c(4\times 2)$ - SO_3 and $p(2\times 2)$ - SO_3 structures. With heating $\text{SO}_2(g)$ evolves from the surface in distinct reaction-limited states at 384 K, 425 K, and 470 K, and the surface reverts to its initially oxidized state. On Cu(110), $\text{SO}_2(g)$ adsorbs molecularly below 300 K; upon annealing to 300 K, the sulfur dioxide disproportionates according to $3\text{SO}_2(a)\rightarrow\text{S}(a)+2\text{SO}_3(a)$ with concomitant desorption of excess $\text{SO}_2(a)$. The surface formed in this manner exhibits large $c(2\times 2)$ -S domains which encompass scattered $c(4\times 2)$ - SO_3 and $p(2\times 2)$ - SO_3 structures in a 1:2 coverage ratio. After being annealed to 400 K, the surface exhibits large $p(2\times 2)$ - SO_3 domains surrounding smaller $c(4\times 2)$ - SO_3 and $c(2\times 2)$ -S islands. Continued heating past 400 K results in decomposition of sulfite according to $\text{SO}_3(a)\rightarrow\text{SO}_2(g)+\text{O}(a)$, evolving sulfur dioxide at 470 K and leaving the surface covered with atomic sulfur and oxygen. Real-time STM images show the mobility of oxygen at island boundaries and the mobility of sulfite amid the $p(2\times 1)$ -O structures. STM measurements suggest that the sulfite occupy four-fold hollow sites. © 2002 American Institute of Physics. [DOI: 10.1063/1.1450545]

I. INTRODUCTION

Sulfur dioxide (SO_2) is infamous for its role as an environmental pollutant. Understanding its interactions with metal surfaces may provide fundamental knowledge useful for the development of catalysts for the reduction of air pollution in industrial and urban settings. Emissions in the United States alone are 1×10^{10} Kg/year, though this figure is down nearly 29% from what it was in the early 90's due to strict emissions regulations.¹ Sulfur dioxide is a major constituent of the flue gas from coal-fired power plants and is readily oxidized by water in the atmosphere into sulfuric acid, which produces acid rain.

In addition to its deleterious environmental effects, by taking up available active sites on metal surfaces, SO_2 , and possibly its decomposition product sulfur, is a well known catalyst poison. Therefore, further advances in our understanding of this interesting molecule and its bonding and reactions with different metals may also aid the production of better flue gas desulfurization units² and help avoid pitfalls in the design of efficient catalysts.

Over the past 20 years the adsorption and reaction of $\text{SO}_2(g)$ has been investigated on a number of single crystal metal surfaces with a number of powerful surface analytical techniques, including x-ray photoelectron spectroscopy (XPS), near-edge x-ray absorption fine structure spectroscopy (NEXAFS), temperature-programmed reaction spectroscopy (TPRS), infrared reflection absorption spectroscopy (IRAS), and, more recently, scanning tunneling microscopy (STM). In general, results suggest that $\text{SO}_2(g)$ adsorption on metal surfaces like Fe, Rh, W, Ni, Pd, Pt, Cu, and Zn is

spontaneous and dissociative, while molecular adsorption dominates on Ag.^{3,4}

Recently, the interaction of $\text{SO}_2(g)$ with the Cu(100) and Cu(110) surfaces has been examined in some detail using XPS, TPRS, and STM. An XPS and TPRS investigation by Polcik *et al.* has indicated that $\text{SO}_2(g)$ dissociates on Cu(100) to yield $\text{SO}(a)$ and $\text{O}(a)$, which are stable up to 300 K, at which temperature $\text{SO}(a)$ and $\text{O}(a)$ recombine to yield $\text{SO}_2(g)$.⁵ In subsequent XPS studies with Cu(100) Ohta *et al.* suggested that $\text{SO}_2(g)$ disproportionates into sulfite (SO_3) and sulfur. NEXAFS studies indicate that the $\text{SO}_3(a)$ coordinates via the S at four-fold hollow sites. From STM results they suggested local distributions of the $\text{SO}_3(a)$ and $\text{S}(a)$ on the surface.⁶ Recently Woodruff *et al.* in their XPS and NEXAFS investigation of the interactions of SO_2 with Cu(111) suggested that $\text{SO}_2(g)$ disproportionates on the surface into sulfur and $\text{SO}_3(a)$. It was further suggested that the sulfite occupies atop sites, oriented with the oxygen atoms pointing toward the surface.⁷

Despite the relatively extensive work on Cu(100) and Cu(111), little has been done to understand how $\text{SO}_2(g)$ interacts with the Cu(110) surface. Recently Pradier *et al.* found using IRAS that in the presence of oxygen $\text{SO}_2(g)$ (600–5400 langmuirs exposure) forms $\text{SO}_3(a)$ and sulfate on the Cu(110) surface at room temperature; on the surface exposed to 200 langmuirs of background oxygen, presumed to form a $c(6\times 2)$ oxygen adlayer, both sulfate and sulfite were observed, the sulfate being the dominant species; on the surface exposed to sufficient oxygen to form a Cu_2O film, sulfite resulted from the reaction with $\text{SO}_2(g)$.⁸ Moreover, it was suggested that in the absence of adsorbed oxygen $\text{SO}_2(g)$ undergoes complete decomposition, presumably into $\text{S}(a)$ and $\text{O}(a)$.

^{a)}Electronic mail: rjm@chemeng.stanford.edu

Despite the conclusions reached by the latter investigation, further work is needed to determine the local distribution of surface species following the interaction of $\text{SO}_2(g)$ with the Cu(110) and Cu(110)- $p(2 \times 1)$ -O surfaces. In this paper we report the results of a coordinated study of the reaction of $\text{SO}_2(g)$ with clean and oxygen-covered Cu(110) by STM, XPS, and TPRS. The mechanism of the reaction and the distribution of structures produced by the reaction products are clarified.

II. EXPERIMENT

Most experiments were performed in an ultrahigh vacuum chamber equipped with STM, low energy electron diffraction (LEED), Auger electron spectroscopy (AES), and temperature-programmed reaction spectroscopy (TPRS). The chamber was equipped with a sputter ion gun and stainless steel gas dosers. The system exhibited a base pressure of 2×10^{-10} Torr following cleaning, which rose to approximately 5×10^{-10} Torr during experiments.

The homemade "Johnnie Walker" type STM employed utilizes RHK STM 100 control electronics and a Pt/Ir tip. The tip was cleaned via induced field evaporation onto a gold surface ($\sim 4 \mu\text{A}$, 15 min) prior to imaging.

Scan dimensions were calibrated using the Cu(110)- $p(2 \times 1)$ -O structure.⁹ All images were processed with x -offset and x -slope subtraction.

The Cu(110) crystal used was aligned to within 0.5° of the (110) plane using Laue backscattering and was mechanically polished down to $0.3 \mu\text{m}$ alumina paste. The crystal was cleaned in vacuum by three Ar ion sputter ($2 \mu\text{A}$, 500 eV, 15 min at 600 K) and anneal (800 K, 10 min) cycles, with the first anneal done in an oxygen atmosphere (1×10^{-7} Torr) to cleanse the surface of impurities observed in STM images. Both sharp $p(1 \times 1)$ LEED patterns and subsequent high-resolution STM images were used to assess the degree of surface cleanliness and order. The crystal could be cooled to 120 K with liquid nitrogen and heated to 1100 K by electron bombardment to the back of the crystal. The temperature was monitored by a Chromel-Alumel thermocouple spot welded to a Ta foil in direct contact with the back of the crystal. The STM ramp housing the crystal and the STM scan head were allowed to thermally equilibrate prior to STM measurements.

Separate XPS and TPRS measurements were made in a second UHV system consisting of interconnected preparation and analysis chambers. The analysis chamber exhibited a base pressure of 3×10^{-10} Torr and was equipped with LEED optics, a Perkin-Elmer 04-548 dual anode x-ray source, an EA-10-plus hemispherical energy analyzer from SPECS, and a UTI 100c quadrupole mass spectrometer (QMS) used for TPRS measurements. The ionizer of the QMS was enclosed in a glass cap with a small hole facing the crystal surface. A computer coupled to the QMS was used to record TPR-spectra. The preparation chamber reached a base pressure of 6×10^{-10} Torr and was equipped with a sputter ion gun and stainless steel gas dosers. The two chambers were isolated from each other during experiments.

In this system the crystal was supported on a Ta foil and heated resistively via two Ta wires spot-welded to the back

of the foil. The temperature was monitored by a Chromel-Alumel thermocouple spot welded to the Ta foil at a location directly behind the crystal. The surface was cleaned by three sputter-anneal cycles, with the first anneal done in an O_2 atmosphere at 10^{-7} Torr. Surface cleanliness and composition were probed with XPS using nonmonochromatic MgK α x-rays. The photoelectrons were collected normal to the surface by the energy analyzer utilizing a 25 eV pass energy. Binding energies were calibrated with respect to the Au 4f peak (84.00 eV) and referenced to the Cu($2p_{3/2}$) peak.

The purity of the $\text{SO}_2(g)$ (Praxair, 99.98%), $\text{O}_2(g)$ ($^{16}\text{O}_2$, Praxair, 99.999%), $^{18}\text{O}_2(g)$ (MSD Isotopes, 97.7%), and $\text{D}_2\text{S}(g)$ (Cambridge Isotope Laboratories, 98%) were monitored with the QMS during dosing; all gases were dosed from the background. Exposures are reported in units of Langmuir ($1 \text{ L} = 10^{-6}$ Torr s). Typical $\text{SO}_2(g)$ dosing pressures were on the order 1×10^{-8} Torr. The $p(2 \times 1)$ oxygen overlayer at 0.24 monolayer (ML) coverage was prepared by dosing 1.5 L (1×10^{-8} Torr, 2.5 min) of $\text{O}_2(g)$ at 450 K, yielding $p(2 \times 1)$ oxygen islands separated by the uncovered Cu surface.

III. RESULTS AND DISCUSSION

A. Surface characterization

1. XPS

XPS measurements following adsorption and reaction of $\text{SO}_2(g)$ with the Cu(110) surface are shown in Fig. 1(a) and summarized in Table I.¹⁰⁻¹⁷ Except for adsorption and measurement at 240 K, all spectra were taken at room temperature following anneal to the specified temperature. An O($1s$) spectrum obtained for a saturated $p(2 \times 1)$ -O overlayer at 0.5 ML coverage and a S($2p$) spectrum obtained for S(a) following decomposition of D_2S are shown at the top of the figure for reference. The position of the sulfur S($2p$) XPS signal is consistent with that observed by Roberts and co-workers in their investigation of $\text{H}_2\text{S}(g)$ reaction on Cu(110).

Due to the absence of a feature for atomic sulfur, the S($2p$) doublet observed following adsorption at 240 K is attributed to molecularly adsorbed SO_2 . The binding energies observed are very close to those previously reported for weak molecular adsorption of SO_2 on Ag(110), but are somewhat different from the measured values for Ni, for which stronger interactions would be expected (Table I). From the molecularly adsorbed state the ratio of the photoionization cross-sections of O($1s$) and S($2p$) was determined to be 1.60, which is within 3% of the theoretical value of 1.64 determined by Scofield.¹⁸ The x-ray photoelectron spectrum of $\text{SO}_2(a)$ does not change significantly with temperature below 300 K.

After the surface is annealed to 324 K the x-ray photoelectron spectrum is marked by the presence of S($2p$) doublets at 161.4 eV and 166.2 eV. The S($2p$) peak at 161.4 eV coincides with that for atomic sulfur, which is evident by comparison to the reference spectrum for S(a) [Fig. 1(a)]. The O($1s$) peak observed after heating to 324 K is shifted by 0.8 eV from that for a $p(2 \times 1)$ oxygen overlayer [Fig. 1(a)]. We attribute this O($1s$) peak and the S($2p$) doublet at 166.2

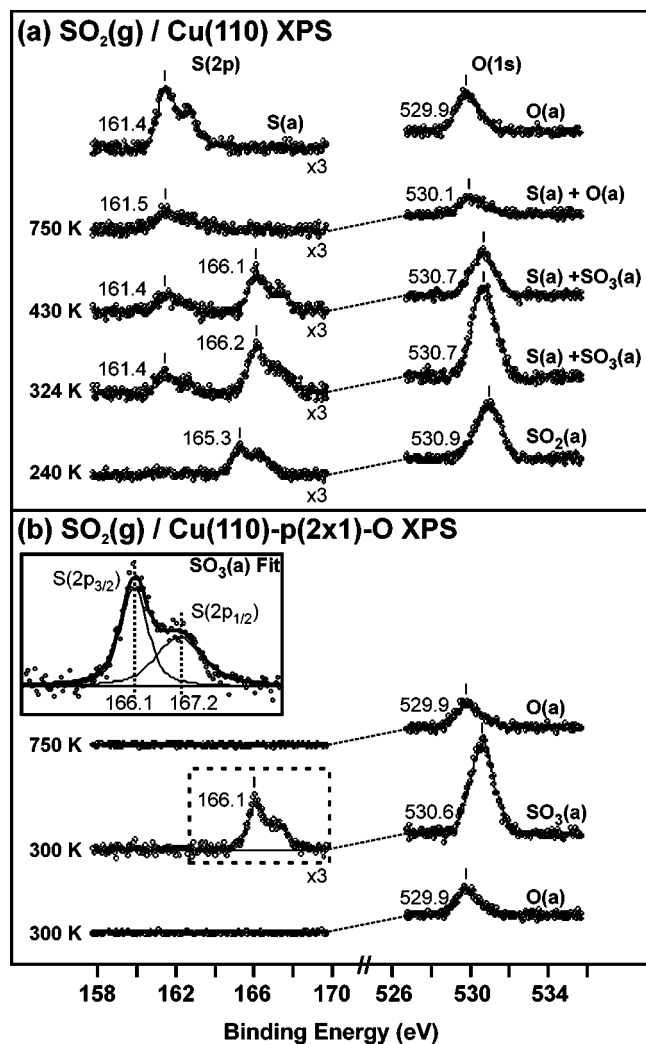
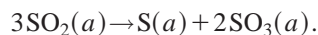


FIG. 1. XPS spectra for (a) SO₂(g) on Cu(110) and (b) SO₂(g) on Cu(110)-*p*(2×1)-O at the indicated temperatures. All S(2*p*) curves are doublets consisting of S(2*p*_{3/2}) and S(2*p*_{1/2}) components approximately 1 eV apart, with the former at lower binding energy. A deconvolution of the SO₃(*a*) S(2*p*) peak (dashed box) is shown in the inset to (b). Binding energies at peak maxima (vertical tick marks) corresponding to S(2*p*_{3/2}) and O(1*s*) peaks have been indicated. Atomic sulfur and oxygen reference spectra for *c*(2×2)-S and *p*(2×1)-O covered surfaces are shown in (a).

eV to an SO_{*x*}(*a*) species. Using the predetermined calibration factor for the oxygen to sulfur ratio, we calculate *x* to be 2.98; the species is SO₃(*a*). The S(2*p*) and O(1*s*) binding energies observed for sulfite agree reasonably well with those reported for SO₃(*a*) on Ag(110) (Table I).

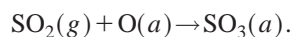
From the S(2*p*) peak areas the ratio of atomic sulfur to SO₃(*a*) is determined to be 1:2, indicating that near 300 K,



Annealing the surface to 430 K does not result in any significant change in binding energies, though there is a decrease in the area of the S(2*p*) feature associated with sulfite and a broadening of the O(1*s*) peak, which, to be discussed shortly, is consistent with the decomposition of SO₃(*a*) into O(*a*) and SO₂(g) in this temperature range. Continued heating to 530 K results in the disappearance of all the sulfite peaks, leaving only atomic sulfur and oxygen on the surface,

as shown by the 750 K scan. The binding energy of the O(1*s*) peak is shifted by 0.2 eV, possibly due to interaction with the sulfur at island boundaries. From the *p*(2×1)-O reference spectrum the coverage of atomic oxygen at 750 K was determined to be 0.23 ML.

X-ray photoelectron spectra for the adsorption and reaction of SO₂(g) with Cu(110)-*p*(2×1)-O are shown in Fig. 1(b) and summarized in Table I. A *p*(2×1)-O overlayer with 0.24 ± 0.06 ML oxygen coverage (as determined by STM images) was prepared by delivery of 1.5 L O₂(g) at 450 K. A 1 L dose of SO₂(g) to this surface at 300 K yielded a spectrum with S2*p* and O(1*s*) peak positions nearly identical to those observed for the sulfite formed on the clean surface [Fig. 1(a)]. This exposure was sufficient to react with all the preadsorbed oxygen (see below), and at room temperature any excess molecular SO₂ desorbed. The oxygen to sulfur ratio was determined to be 3.03, as expected for SO₃(*a*). Therefore we conclude that at 300 K on Cu(110)-*p*(2×1)-O sulfur dioxide reacts stoichiometrically with adsorbed oxygen to form sulfite according to



Annealing this surface beyond 530 K leads to the reversible loss of sulfite, leaving the initial 0.24 ML of atomic oxygen on the surface, as shown by the x-ray photoelectron spectrum taken after the anneal to 750 K [Fig. 1(b)].

2. Temperature-programmed reaction spectroscopy

Following adsorption of SO₂(g) on Cu(110), SO₂(g) evolves at 333 K and 470 K upon heating [Fig. 2(a)]. For the temperature-programmed reaction spectrum shown in Fig. 2(a) the surface was exposed to 0.05 L SO₂(g) at 250 K and heated to 750 K. No increase in area of either peak was observed following an exposure of SO₂(g) twice this amount. The TPRS are interpreted as the molecular desorption of SO₂(g) centered at 333 K followed by a reaction-limited evolution centered at 470 K. This interpretation is supported by the XPS results discussed above. Assuming a first order pre-exponential factor of 1 × 10¹³ s⁻¹, we estimate the activation energy for desorption at 470 K to be 31 kcal/mol. No other species were observed to desorb.

Temperature-programmed reaction spectra following the adsorption of SO₂(g) on Cu(110)-*p*(2×1)-O reveal the molecular desorption peak centered at 333 K and peaks centered at 384 K, 425 K, and 470 K [Fig. 2(b)]. Using a pre-exponential factor of 1 × 10¹³ s⁻¹, we estimate the activation energy for the formation of each of these reaction-limited states to be 25 kcal/mol (384 K), 28 kcal/mol (425 K), and 31 kcal/mol (470 K). With increasing exposure, states were seen to populate and saturate sequentially beginning with the peak at the highest temperature.

Experiments using isotopically labeled oxygen suggest that the sulfite species has monodentate coordination to the surface [Fig. 2(c)]. Initially ¹⁸O₂ was used to prepare the Cu(110)-*p*(2×1)-¹⁸O surface, and SO₂(g) was introduced at 320 K to yield the sulfite-covered surface. Of the possible isotopes for sulfur dioxide which could evolve upon heating, only mass-to-charge ratios of 64 (SO₂) and 66 (SO¹⁸O) were detected; S¹⁸O¹⁸O could not be detected. Previous investiga-

TABLE I. Summary of the XPS binding energies (eV) observed in this work (row 2, first entry). Those reported in other (relevant) investigations have been shown for comparison. S(2*p*) binding energies correspond to the S(2*p*_{3/2}) signal. Unavailability of experimental data is indicated by a horizontal dash.

	S		SO ₂		SO ₃		SO ₄	
	S(2 <i>p</i>)	O(1 <i>s</i>)	O(1 <i>s</i>)	S(2 <i>p</i>)	O(1 <i>s</i>)	S(2 <i>p</i>)	O(1 <i>s</i>)	S(2 <i>p</i>)
Gas (Ref. 11)	-	-	539.8	174.8	540.7	176.7	-	-
Cu(110)	161.4	529.9	530.9	165.3	530.7	166.1	-	-
Cu(110) (Ref. 10)	161.3							
Cu ₂ S (Ref. 12)	161.3	-	-	-	-	-	-	-
CuO (Ref. 12)	-	529.7	-	-	-	-	-	-
CuSO ₄ (Ref. 13)	-	-	-	-	-	-	532.2	169.5
Ag(110) (Ref. 14)	-	528.4	530.6	165.4	530.2	166.1	530.6	167.9
Ag(111) (Ref. 15)	161.8	-	-	-	-	-	531.3	168.4
Ag ₂ S (Ref. 16)	161.6	-	-	-	-	-	-	-
Ag foil (Ref. 17)	-	528.3	-	-	-	-	-	-
Ni (Ref. 12)	-	-	531.2	165.8	-	-	-	-

tors have suggested that sulfite coordinates to Ag(110) through either one (monodentate) or two oxygen atoms (bidentate)¹⁹ and to Cu(100) or Cu(111) by three oxygen atoms.^{6,7} Assuming the O-metal bonds to be equivalent and

to be *intraconvertible* among the other S–O bonds, the latter two species would yield peak area ratios SOO to SO¹⁸O of one to two, respectively. With the same assumptions the monodentate sulfite formed by the addition of SO₂(*g*) to the surface containing preadsorbed ¹⁸O would yield an infinite ratio of SOO to SO¹⁸O, as it is based solely on the probability of breaking and making *inconvertible* O–Cu bonds. The observed ratio of the peak areas of approximately ten to one is indicative of the dominance of a monodentate sulfite which decomposes primarily by cleavage of the S–O bond.

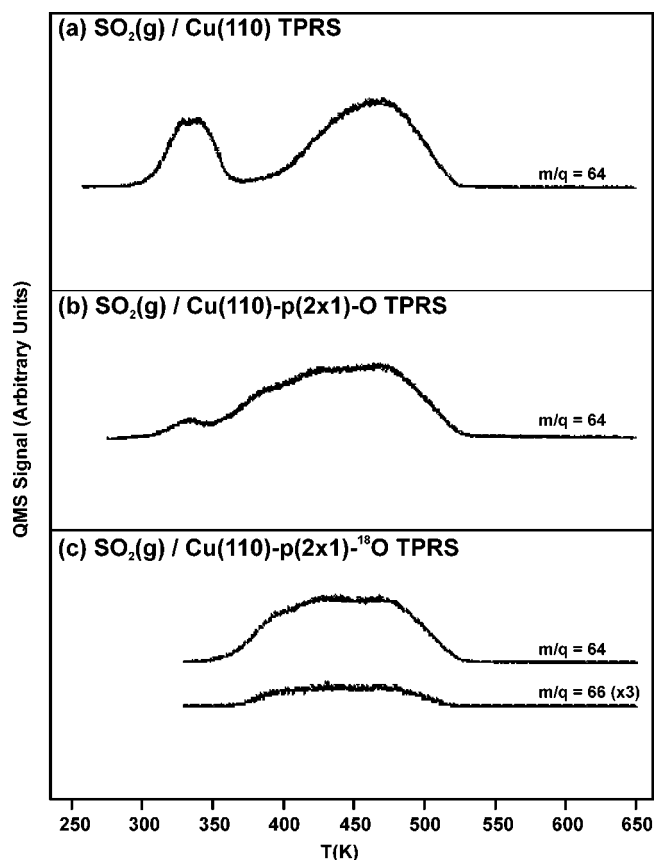
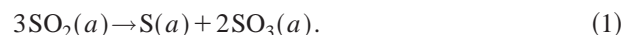


FIG. 2. TPRS spectra for (a) SO₂(*g*) on Cu(110), (b) SO₂(*g*) on Cu(110)-*p*(2×1)-O, and (c) SO₂(*g*) on Cu(110)-*p*(2×1)-¹⁸O. The average heating rate was 0.7 K/s. The vertical axis corresponds to the QMS signal for the species with the indicated mass to charge (*m/q*) ratio.

3. Reaction summary

Below room temperature SO₂(*g*) adsorbs molecularly (Fig. 1) without any significant decomposition, i.e., SO₂(*g*) → SO₂(*a*). Upon heating SO₂(*a*) disproportionates into sulfur and sulfite [Fig. 1(a)] and excess SO₂ desorbs [Fig. 2(a)]



Because SO₂ reacts stoichiometrically with preadsorbed oxygen, we propose that a fraction of the SO₂(*a*) population undergoes complete decomposition through a series of elementary surface reactions, and the oxygen which is liberated reacts with SO₂(*a*) to form SO₃(*a*):



This reaction sequence gives the overall stoichiometry observed. The fact that SO(*a*) was not observed with XPS suggests that the rate of SO(*a*) decomposition [Eq. (2b)] is faster than that for the decomposition of SO₂(*a*) [Eq. (2a)].

The sulfite formed on the clean surface is stable up to 400 K, at which temperature its decomposition is marked by a broad SO₂(*g*) peak in TPRS centered at 470 K [Fig. 2(a)]:

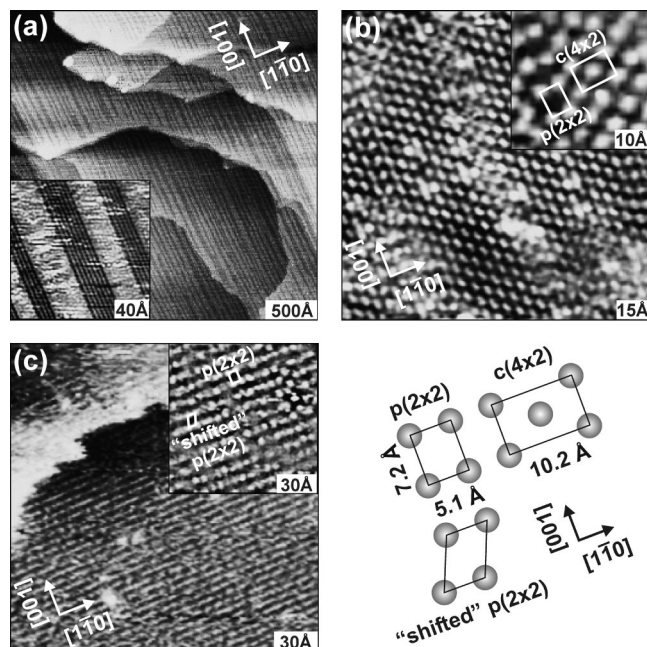


FIG. 3. STM images of (a) a $p(2\times 1)$ -O covered surface at 0.24 ML oxygen coverage, with the inset showing the surface at higher resolution; tunneling conditions: 97.4 mV, 0.30 nA and inset, -405 mV, 0.68 nA (constant height). (b) $\text{SO}_3(a)$ covered surface following $\text{SO}_2(g)$ dose onto the surface in (a) at 300 K, with $c(4\times 2)$ and $p(2\times 2)$ structures indicated in the inset; tunneling conditions: -251 mV, 0.57 nA (constant height) and inset, -111 mV, 1.31 nA (constant height). (c) $\text{SO}_3(a)$ covered surface following $\text{SO}_2(g)$ dose onto the surface in (a) at 400 K, with $p(2\times 2)$ and "shifted" $p(2\times 2)$ structures indicated in the inset; tunneling conditions: -0.56 V, 0.55 nA and inset, -453 mV, 0.53 nA (constant height). The accompanying model, with dimensions consistent with STM measurements, depicts the $p(2\times 2)$ and $c(4\times 2)$ - SO_3 structures appearing in (b) as well as the "shifted" $p(2\times 2)$ - SO_3 structure in (c).



The $p(2\times 1)$ -O overlayer shifts the surface chemistry away from the decomposition pathway. At 300 K $\text{SO}_2(g)$ reacts stoichiometrically with atomic oxygen to yield sulfite [Fig. 1(b)]:



This sulfite species is stable up to 350 K, at which temperature the reaction limited evolution of $\text{SO}_2(g)$ from states with peaks centered at 384 K, 425 K, and 470 K [Fig. 2(b)] results in the conversion of the surface back to its initially oxidized state [cf. Eq. (4)].

B. Local structure

1. $\text{SO}_2(g)$ on Cu(110)- $p(2\times 1)$ -O

The initial state of this surface consisted of islands of Cu-O chains running along the [001] direction, each row spaced by two lattice distances along the $[1\bar{1}0]$ direction, the islands being separated by regions of uncovered surface [Fig. 3(a)].²⁰ The coverage of oxygen on this surface was approximately 0.24 ML.

$\text{SO}_2(g)$ reacts with this $p(2\times 1)$ -O overlayer to yield a surface covered with $c(4\times 2)$ and $p(2\times 2)$ structures [Fig. 3(b)]. All oxygen rows react away. The $c(4\times 2)$ structure forms large domains, while the $p(2\times 2)$ is scattered in much

smaller islands. This STM result is consistent with the streaky $c(4\times 2)$ LEED pattern observed. The species comprising the $c(4\times 2)$ and $p(2\times 2)$ structures have identical corrugation. Since this surface species was identified as sulfite by XPS [Fig. 1(b)], we interpret the $c(4\times 2)$ and $p(2\times 2)$ structures as $\text{SO}_3(a)$ domains.

The formation of the $c(4\times 2)$ structure may be driven by repulsive lateral interactions within the sulfite overlayer. This $c(4\times 2)$ - SO_3 structure can be formed by shifting alternate rows of the $p(2\times 2)$ structure by one lattice unit along the [001] azimuth (Fig. 7). The distance between sulfite nearest neighbors in the $c(4\times 2)$ structure is 6.24 Å, compared to the nearest neighbor distance of 5.1 Å in the $p(2\times 2)$. The local coverage of sulfite in both the $c(4\times 2)$ and $p(2\times 2)$ structures is 0.25 ML. This coverage is close to the initial 0.24 ML oxygen coverage, and it would be expected to result from the stoichiometric reaction of sulfur dioxide and preadsorbed oxygen. A two-dimensional model with dimensions consistent with STM measurements is shown (Fig. 3).

For the surface prepared by dosing $\text{SO}_2(g)$ onto the partially oxidized surface at 400 K, the $p(2\times 2)$ - SO_3 structure dominates the surface [Fig. 3(c)]. This fact is reflected by the streaky $p(2\times 2)$ LEED pattern observed. A higher resolution scan of the surface (inset) shows $p(2\times 2)$ and "shifted" $p(2\times 2)$ structures, similar to the $p(3\times 2)$ and "shifted" $p(3\times 2)$ - CO_2 structures observed on Ag(110).²¹ The shifted structures, which require alternate rows of sulfite to shift along the $[1\bar{1}0]$ direction by one lattice unit, may arise from mobility of the sulfite species along the $[1\bar{1}0]$ direction. They appear as defects in the large domains of the $p(2\times 2)$ structure.

2. $\text{SO}_2(g)$ on Cu(110)

STM reveals three local structures that result from the exposure of the clean Cu(110) surface to $\text{SO}_2(g)$: $c(2\times 2)$, $c(4\times 2)$, and $p(2\times 2)$ [Fig. 4(a)]. The $c(2\times 2)$ structures form large islands, while the $c(4\times 2)$ and $p(2\times 2)$ structures are dispersed randomly throughout the scan area into much smaller domains, approximately three to four unit cells wide along the $[1\bar{1}0]$. The LEED pattern observed for this surface is a $c(2\times 2)$, in agreement with the STM images, as islands of this structure dominate the scan area. The corrugation of the species comprising the $c(2\times 2)$ domains is different from that of the $c(4\times 2)$ and $p(2\times 2)$ structures. As discussed above (Sec. III B 1), the $c(4\times 2)$ and $p(2\times 2)$ structures are attributed to sulfite.

STM and LEED results for the decomposition of $\text{D}_2\text{S}(g)$ on Cu(110) suggest that the $c(2\times 2)$ structures observed in Fig. 4(a) are due to sulfur [Fig. 4(b)]. $\text{D}_2\text{S}(g)$ is expected to decompose into $\text{D}_2(g)$ and $c(2\times 2)$ -S,¹⁴ and the corrugation of the $c(2\times 2)$ -S structure is identical to that observed for the $c(2\times 2)$ structure formed in the disproportionation of $\text{SO}_2(g)$ [Eq. (1)]. The $c(2\times 2)$ -S domains in Fig. 4(b) are separated by streaky anti-phase domain boundaries, where the sulfur adatoms have a mobility too large to be imaged by the STM at the scan speed used. An area calculation [Fig. 4(c), bottom] for a typical scan area [Fig. 4(c) top] shows that the coverage of $c(2\times 2)$ -S (dark patches) is 18.0%. Av-

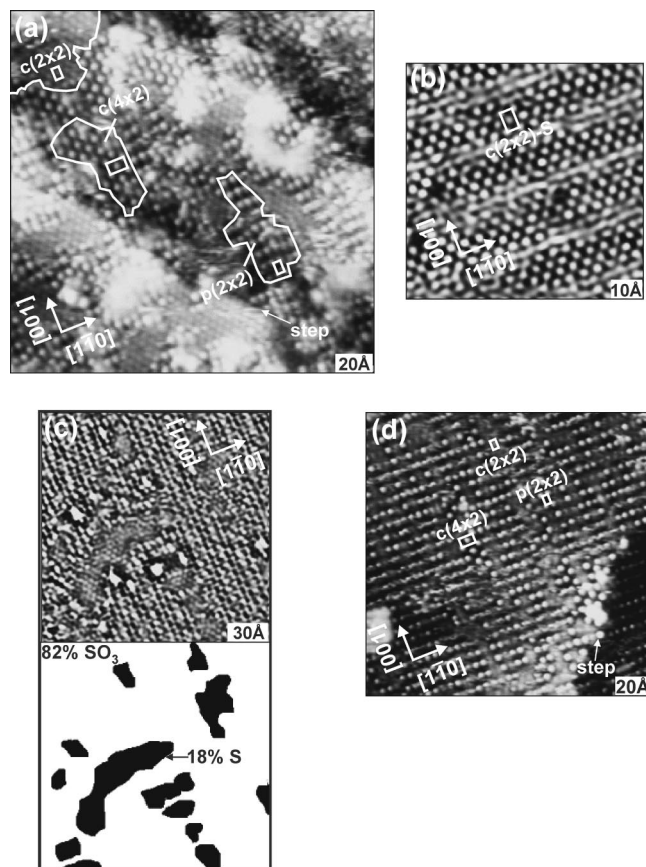


FIG. 4. STM images of (a) $\text{SO}_2(\text{g})$ on $\text{Cu}(110)$, showing large $c(2 \times 2)$ domains and scattered $p(2 \times 2)\text{-SO}_3$ and $c(4 \times 2)\text{-SO}_3$ structures; tunneling conditions: -1.52 V, 0.52 nA. (b) $\text{D}_2\text{S}(\text{g})/\text{Cu}(110)$, showing $c(2 \times 2)\text{-S}$ structures separated by streaky anti-phase domain boundaries; tunneling conditions: -0.50 V, 1.23 nA (constant height). From this image it is determined that the $c(2 \times 2)$ structures following $\text{SO}_2(\text{g})$ adsorption (a) are due to sulfur. (c) The top image is an STM scan of the $\text{Cu}(110)$ surface following disproportionation of $\text{SO}_2(\text{g})$ into sulfite and sulfur structures at 300 K, where the sulfite domains surround sulfur islands of lower corrugation; tunneling conditions: -343 mV, 0.49 nA (constant height). The bottom image corresponds to the STM scan above, where it is calculated that the sulfite structures (white area) cover 82% of the surface and the sulfur domains (black patches) the remaining 18% . An average coverage weighted sulfite to sulfur area ratio of $2:1$ is obtained from similar images, which is consistent with the $2:1$ sulfite to sulfur ratio determined by XPS. (d) $\text{SO}_2(\text{g})$ on $\text{Cu}(110)$ at 400 K, showing large $p(2 \times 2)\text{-SO}_3$ islands surrounding scattered $c(4 \times 2)\text{-SO}_3$ and $c(2 \times 2)\text{-S}$ domains; tunneling conditions: 0.56 V, 0.66 nA.

eraging over 15 scan regions approximately the same size as that in Fig. 4(c) (top) gives $20.53\% \pm 1.53\%$, giving a area weighted coverage of S of 0.1 ML. Similarly, the sulfite coverage can be determined to be 0.2 ML. Thus, the sulfite to sulfur ratio determined by STM is $2:1$, in accordance with the XPS findings [Eq. (1)].

Introducing $\text{SO}_2(\text{g})$ at 400 K, a temperature at which some decomposition of sulfite can occur, produces a surface with a dominant $p(2 \times 2)$ structure with a few scattered $c(2 \times 2)$ and $c(4 \times 2)$ defects [Fig. 4(d)]. The prevalence of the $p(2 \times 2)$ structure is similar to what was observed for sulfite on the oxygen covered surface at 400 K [Fig. 3(c)]. The $p(2 \times 2)$ LEED pattern for this surface is consistent with this being the dominant structure on the surface. The $p(2 \times 2)\text{-SO}_3$ areas appear to be separated by small (dim) do-

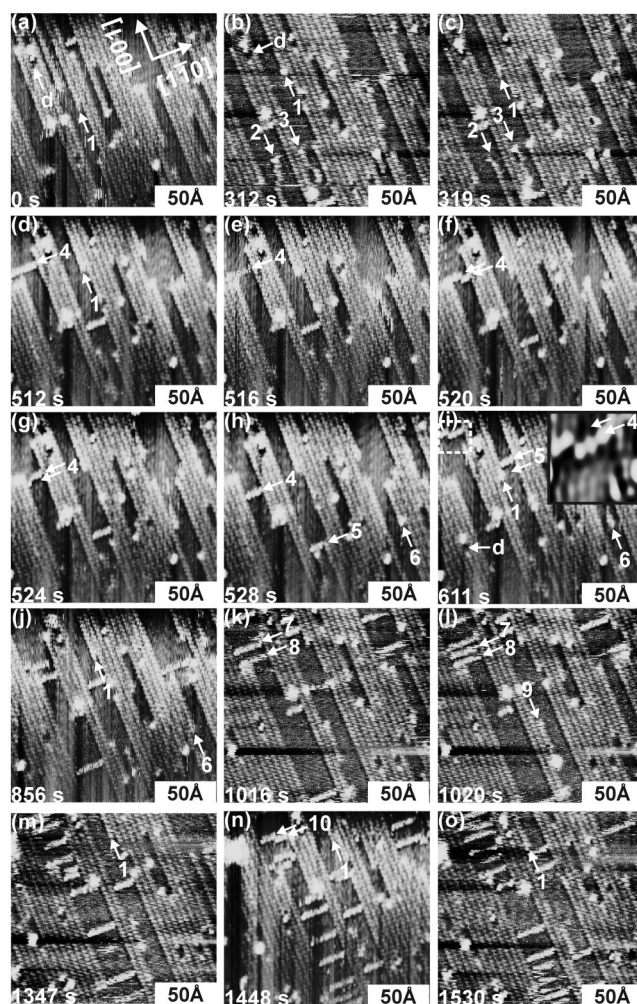


FIG. 5. A selection of STM images obtained at $2\text{--}3$ s/frame during $\text{SO}_2(\text{g})$ dosing onto a $\text{Cu}(110)\text{-}p(2 \times 1)\text{-O}$ surface at 0.24 ML oxygen coverage; tunneling conditions: -135 mV, 0.54 nA (constant height). The time of each frame (lower right) is in reference to that at zero seconds (s) (frame a). Rows orthogonal to the oxygen structures appear and grow in number with time (frames a–o). They display two-fold spacing in the $[001]$ (frame 1, arrows 7 and 8) and $[1\bar{1}0]$ directions (frame i, inset, arrow 4) and are interpreted as sulfite structures, identical to those comprising the $p(2 \times 2)\text{-SO}_3$ structures [Figs. 3(c) and 4(d)]. The inset to frame i is an enlargement of the boxed area shown at the upper left hand corner of the frame. The arrows correspond to features described in the text. See <http://www.stanford.edu/group/madix> for a video clip.

main of lower corrugation, which we interpret as $c(2 \times 2)\text{-S}$ structures. There is apparently a significant rearrangement of the surface structure from that at 300 K [Fig. 4(a)], since the large $c(2 \times 2)\text{-S}$ domains have dissipated. A $c(4 \times 2)\text{-SO}_3$ structure has been indicated in the figure and is seen to sit in-between $p(2 \times 2)$ domains.

3. Real-time imaging: $\text{SO}_2(\text{g})$ on 0.24 ML $p(2 \times 1)\text{-O}$

Real-time STM images show the mobility of sulfite and oxygen rows during reaction of $\text{SO}_2(\text{g})$ with preadsorbed oxygen at 300 K (Figs. 5 and 6). The $\text{Cu}(110)$ surface was initially prepared with a $p(2 \times 1)\text{-O}$ overlayer at 0.24 ML coverage [Fig. 3(a)], and sulfur dioxide was dosed at a pressure of 1×10^{-9} Torr. A specific area with well-defined fea-

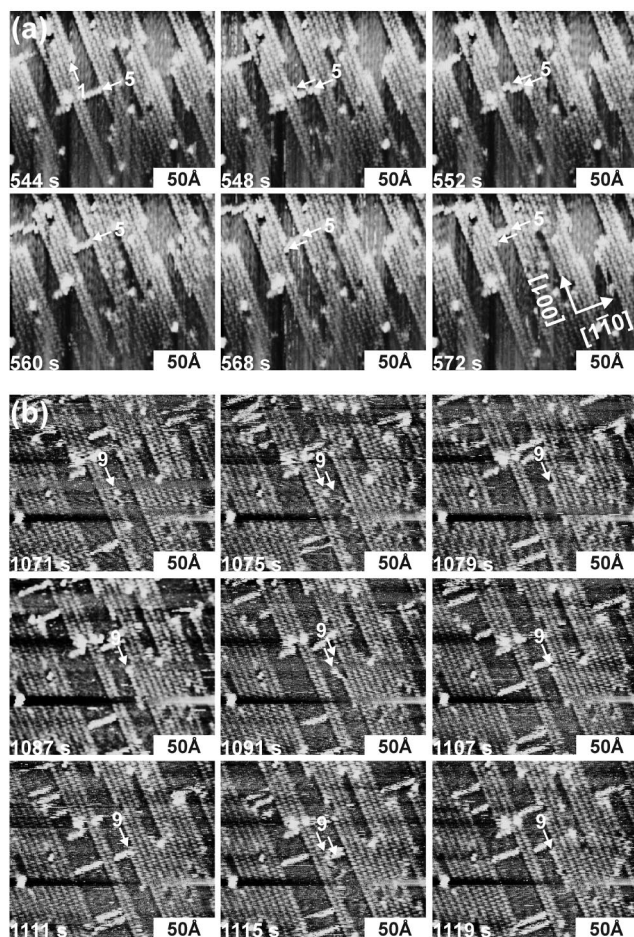


FIG. 6. A selection of STM images obtained at 2–3 s/frame during $\text{SO}_2(g)$ dosing onto a $\text{Cu}(110)\text{-}p(2\times 1)\text{-O}$ surface at 0.24 ML oxygen coverage; tunneling conditions: -135 mV, 0.54 nA (constant height). The time of each frame (lower right) is in reference to that at zero seconds (s) in Fig. 5(a). (a) Sequence of images accompanying Fig. 5(h), demonstrating the snakelike migration of a sulfite row (arrow 5) and subsequent collision with an oxygen row (arrow 1). After collision at 560 s, a portion of the sulfite row is left behind. (b) Sequence of STM images shortly following Fig. 5(l), showing the snakelike migration of an oxygen row (arrow 9) from one $p(2\times 1)\text{-O}$ island to another, apparently involving reptilation (see text).

tures was tracked at a scan rate between 2–3 s/frame. $\text{Cu}\text{-O}$ rows in the $p(2\times 1)$ islands, separated by regions of clean surface are clearly visible in Fig. 5(a).

This time sequence reveals several interesting features of the reaction. Rows of oxygen at the edges of the $p(2\times 1)\text{-O}$ islands are mobile, consistent with the heightened reactivity of oxygen at island edges.²² This behavior is demonstrated by row 1 in Fig. 5(b) and 5(o) and row 6 in Figs. 5(h)–5(j), which show the oxygen rows moving from one $p(2\times 1)\text{-O}$ island to another. Further inspection reveals that the rows of oxygen translate from one island to another in a “snakelike” fashion. This behavior can be seen in Figs. 5(b) and 5(c) (arrows 2 and 3) and Fig. 6(b) (arrow 9). At first a small segment of the chain moves laterally, and the remainder follows shortly thereafter, apparently involving reptilation. The migration of $p(2\times 1)\text{-O}$ segments has been observed previously by Besenbacher and co-workers, who calculated an effective diffusion coefficient $D \geq 10^{-13}$ cm^2/s .²⁰

As reaction proceeds, increasing numbers of short, bright rows, oriented along the $[1\bar{1}0]$ direction appear, spanning the space between the $p(2\times 1)\text{-O}$ islands. These features have the same corrugation as the features in the $p(2\times 2)\text{-SO}_3$ structures discussed above [Figs. 3(c) and 4(d)]. In Fig. 5(i) (arrow 4, inset) these chains can be seen to consist of units with two-fold spacing along the $[1\bar{1}0]$ direction. Furthermore, at closest approach the rows exhibit a two-fold spacing along the $[001]$ direction (see below). Thus they appear to form a local $p(2\times 2)$ configuration like those of sulfite discussed above. Hence we interpret these rows as sulfite structures. Lateral interactions prevent these rows from approaching one another more closely than 7.2 Å, which corresponds to two unit cell vectors along the $[001]$ direction of the underlying copper surface.

The mobility of sulfite is appreciable along the $[001]$ azimuth. When viewed continuously, the motion of the sulfite rows up and down the channels separating the oxygen islands appears random, suggesting little interference by the STM. However, they do migrate together to form transient, rudimentary $p(2\times 2)$ structures [Figs. 5(k) and 5(i), arrows 7 and 8]. Attractive interactions (along the $[1\bar{1}0]$ direction) keep these rows intact, but random migration leads to separation of the rows forming the $p(2\times 2)$ structure.

Fragmentation of an $\text{SO}_3(a)$ row accompanied by a shift of one lattice unit in the $[001]$ direction would lead to a rudimentary $c(4\times 2)$ structure, and there is indication of such behavior in Figs. 5(f) and 5(g) (arrow 4) and Fig. 5(h) (arrow 10). The two portions of the fragmented rows appear to interact with the adjoining oxygen islands, resulting in a “snakelike” migration of the sulfite structure, through this intermediate structure along the $[001]$ as shown by arrow 5 in Fig. 6(a). Their translation is seen to take place in steps in that one portion of the row moves first and is subsequently followed by the remainder, similar to the mechanism by which rows of oxygen translate from one $p(2\times 1)\text{-O}$ island to another.

There are also numerous examples of the fracture of sulfite rows caused by the collision of a migrating sulfite row with a narrowing of the space between the oxygen islands. This is shown in Figs. 5(d)–5(h) (arrow 4) and further demonstrated in Fig. 6(a) (arrow 5), in which the sulfite row (arrow 5) is split into two segments following collision with an oxygen row (arrow 1).

4. Binding sites and two-dimensional model

A partial coverage of sulfite on the $p(2\times 1)\text{-O}$ surface was created in order to determine the binding site of $\text{SO}_3(a)$.²³ The surface was initially prepared with a $p(2\times 1)\text{-O}$ overlayer at 0.24 ML coverage. $\text{SO}_2(g)$ and $\text{O}_2(g)$ were subsequently co-dosed to produce the surface shown in Figs. 7(a) and 7(b). Figures 7(a) and 7(b) show atomically resolved $\text{Cu}\text{-O}$ rows in their $p(2\times 1)$ arrangement and sulfite moieties between the islands appear as bright circular features. The sulfites are arranged in both $c(4\times 2)$ and $p(2\times 2)$ structures, though defects (*d*) are evident. These defects may result from the inability of the sulfite rows to shift to the $c(4\times 2)$ structure due to lateral interactions with adjacent

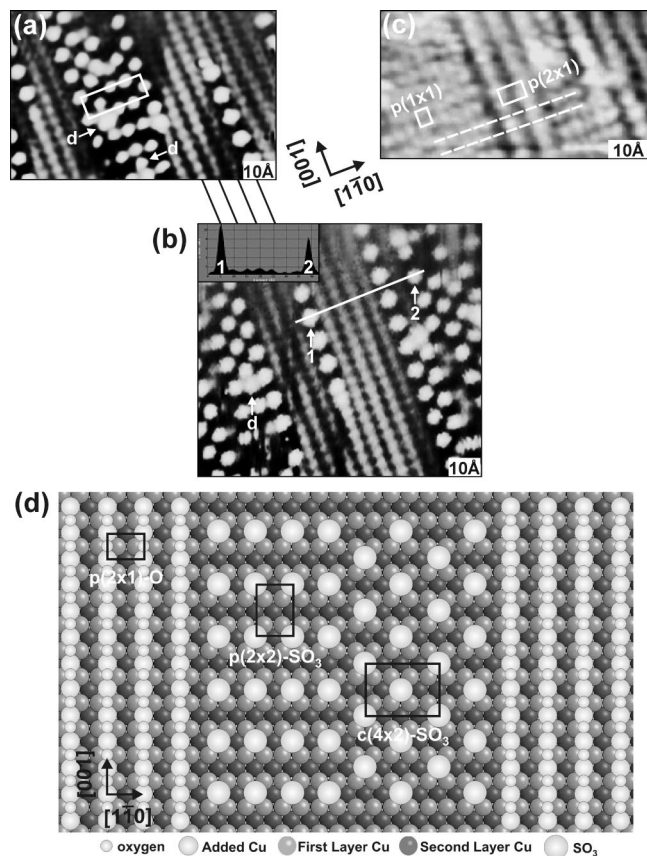


FIG. 7. STM images of (a) and (b) $\text{SO}_2(g) + \text{O}_2(g)$ co-dosed onto a $\text{Cu}(110)-p(2 \times 1)-\text{O}$ surface at 0.24 ML coverage; tunneling conditions: (a) -415 mV, 0.25 nA (constant height) and (b) -416 mV, 0.60 nA (constant height). (a) and (b) are of the same general area, the solid lines connect corresponding $p(2 \times 1)-\text{O}$ and sulfite rows. The solid line in (b) accompanies the line scan shown in the inset; arrows 1 and 2 correspond to the sulfite features indicated in the line scan. (c) A surface with $p(2 \times 1)-\text{O}$ rows amid the $\text{Cu}(110)-p(1 \times 1)$ lattice; tunneling conditions: -98.4 mV, 0.60 nA (constant height). The dashed lines, corresponding to rows of Cu atoms oriented along the $[1\bar{1}0]$, are seen to sit in-between bright features comprising the $p(2 \times 1)$ structure, suggesting that the species imaged by the STM in the $p(2 \times 1)-\text{O}$ overlayer are the “added” Cu atoms. (d) A structural model consistent with line-scan measurements in (a) and (b), where it is proposed that the sulfites comprising the $p(2 \times 2)$ and $c(4 \times 2)$ structures occupy four-fold hollow sites.

sulfite and oxygen structures. The line scan in Fig. 7(b) (inset) shows the corrugation of the sulfites (arrows 1 and 2) relative to the species comprising the $p(2 \times 1)$ structure.

In order to determine the binding site of sulfite the entity imaged in the $\text{Cu}-\text{O}$ islands must be first determined so that it can be used as a reference point for the sulfite. The STM scan shown in Fig. 7(c) suggests that the species imaged in the $p(2 \times 1)$ structures are the “added” Cu atoms. Indicated in the figure are $p(1 \times 1)$ and $p(2 \times 1)$ unit cells. The $p(1 \times 1)$ is due to the $\text{Cu}(110)$ rectangular lattice and we assume that it is due to the imaging of Cu atoms.

Results of previous studies suggest that the $p(2 \times 1)-\text{O}$ structure results from the sequential addition of oxygen atoms to long bridge sites and Cu atoms to four-fold hollow sites along the $[001]$ azimuth.^{9,20} According to Fig. 7(c), lines extended through the close-packed rows of Cu atoms (dashed lines) oriented along the $[1\bar{1}0]$ direction straddle the

brighter $p(2 \times 1)$ features in the oxide island, as expected if copper atoms are imaged in the oxide islands. We thus conclude that we have imaged the copper atoms in the oxygen islands. This result agrees well with previous work.²⁴

With the location of the copper in the $p(2 \times 1)$ image of the oxide island known, the binding site of sulfite was straightforwardly determined to be the four-fold hollow using the line scan in Fig. 7(b); it is consistent with the registry of the sulfites (arrows 1 and 2) relative to adjacent $p(2 \times 1)$ rows [Fig. 7(b)]. The edge of the sulfite domain begins with the four-fold hollow site next nearest to the oxygen island edge (along the $[1\bar{1}0]$ direction), not the adjacent four-fold hollow site. A four-fold hollow binding site configuration does not preclude the possibility, however, of the incorporation of an “added” Cu atom into the resulting sulfite structure following reaction between $\text{SO}_2(g)$ and $\text{O}(a)$ [Eq. (5)]. From the sulfite binding site it follows that the sulfur atoms observed on the clean surface [Fig. 4(a)] formed by the disproportionation of $\text{SO}_2(a)$ [Eq. (1)] also occupy four-fold hollows. This is in agreement with the binding site as suggested by King and co-workers.²⁵

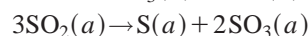
5. Nucleation and growth of $\text{SO}_3(a)$ structures

The pattern of growth of sulfide and sulfite following the exposure of $\text{Cu}(110)$ to $\text{SO}_2(g)$ suggests certain qualitative features of the growth process. The basic observation is that sulfite forms $c(4 \times 2)$ and $p(2 \times 2)$ patches around $c(2 \times 2)-\text{S}$ islands. Following decomposition of $\text{SO}_2(a)$ into sulfur and oxygen [Eq. (2)], $\text{SO}_2(g)$ reacts rapidly with the oxygen adatoms to form sulfite. During this process sulfur and sulfite segregate into patches of $c(2 \times 2)$, $p(2 \times 2)$, and $c(4 \times 2)$ structures [Figs. 4(a) and 4(c)]. The $c(2 \times 2)-\text{S}$ domains apparently prevent sulfite from relaxing into the $c(4 \times 2)$ configuration.

On the $\text{Cu}(110)-p(2 \times 1)-\text{O}$ surface the nucleation and growth of the $c(4 \times 2)$ and $p(2 \times 2)$ sulfite structures at $p(2 \times 1)-\text{O}$ island boundaries is apparently accompanied by a $p(2 \times 2) \rightarrow c(4 \times 2)$ structural relaxation. A minor amount of the $p(2 \times 2)$ structure can result from a one lattice unit mismatch of nucleation sites of the $c(4 \times 2)$ structure along the $[001]$ direction at two adjacent oxygen structures, as indicated by the boxed area in Fig. 7(a). Shown, for example, is a full $c(4 \times 2)$ unit cell with an adjacent half unit cell at opposite sides of a region separating two oxygen islands; a domain boundary between these two structures forms a chain of $p(2 \times 2)$ cells running along the $[001]$ direction. Lateral sulfite-sulfite and sulfite-oxygen forces appear to pin the $p(2 \times 2)$ structure and prevent its relaxation into the $c(4 \times 2)$. This effect leads to a mixture of sulfite moieties amid the $p(2 \times 1)-\text{O}$ structures [Figs. 7(a) and 7(b)].

IV. SUMMARY

- (1) On the $\text{Cu}(110)$ surface $\text{SO}_2(g)$ adsorbs molecularly below 300 K. Heating the surface to 300 K results in the disproportionation of a fraction of the $\text{SO}_2(a)$ population into $\text{SO}_3(a)$ and $\text{S}(a)$:



The surface is covered by large $c(2 \times 2)$ -S and scattered $c(4 \times 2)$ -SO₃ and $p(2 \times 2)$ -SO₃ structures.

- (2) Disproportionation at 300 K is concomitant with the desorption of excess SO₂(*a*). Continued heating to 400 K yields a surface covered with $p(2 \times 2)$ -SO₃ and scattered $c(2 \times 2)$ -S and $c(4 \times 2)$ -SO₃ structures. Further heating leads to the decomposition of sulfite at 470 K according to $\text{SO}_3(a) \rightarrow \text{SO}_2(g) + \text{O}(a)$, which is complete by 530 K, yielding a surface covered with atomic sulfur and oxygen.
- (3) On the Cu(110)- $p(2 \times 1)$ -O surface SO₂(*g*) reacts according to $\text{SO}_2(g) + \text{O}(a) \rightarrow \text{SO}_3(a)$ at 300 K to yield a surface covered with $c(4 \times 2)$ -SO₃ and scattered $p(2 \times 2)$ -SO₃ structures.
- (4) Real-time image sequences show the mobility of oxygen at $p(2 \times 1)$ -O island boundaries and the mobility of sulfite amid the oxygen structures.
- (5) Sulfite and sulfur occupy four-fold hollow binding sites. TPRS measurements with isotopically labeled oxygen indicate that sulfite coordinates as a monodentate species.
- (6) On the oxygen covered surface, SO₂(*g*) is oxidized at $p(2 \times 1)$ -O island boundaries into $p(2 \times 2)$ -SO₃ and $c(4 \times 2)$ -SO₃ structures. A one lattice unit mismatch (along the [001]) of nucleation sites at opposing $p(2 \times 1)$ -O islands leads to the $p(2 \times 2)$ structure at $c(4 \times 2)$ domain boundaries. Once all of the oxygen has been reacted away, relaxation of the sulfites yields a $c(4 \times 2)$ -SO₃ covered surface.

ACKNOWLEDGMENT

We gratefully acknowledge the National Science Foundation (NSF CHE 9820703) for support of this work.

- ¹EPA, <http://www.epa.gov> (2000).
- ²C. D. Cooper and F. C. Alley, *Air Pollution Control: A Design Approach*, 2nd ed. (Waveland, Prospect Heights, IL, 1994).
- ³J. Haase, *J. Phys.: Condens. Matter* **9**, 3647 (1997).
- ⁴H. W. Wassmuth, J. Ahner, M. Hofer, and H. Stolz, *Prog. Surf. Sci.* **42**, 257 (1993).
- ⁵M. Polcik, L. Wilde, J. Haase, B. Brena, D. Cocco, G. Comelli, and G. Paolucci, *Phys. Rev. B* **53**, 13720 (1996).
- ⁶T. Nakahashi, S. Terada, T. Yokoyama, H. Hamamatsu, Y. Kitajima, M. Sakano, F. Matsui, and T. Ohta, *Surf. Sci.* **373**, 1 (1997).
- ⁷G. J. Jackson, S. M. Driver, D. P. Woodruff, N. Abrams, R. G. Jones, M. T. Butterfield, M. D. Crapper, B. C. C. Cowie, and V. Formoso, *Surf. Sci.* **459**, 231 (2000).
- ⁸C. M. Pradier and P. Dubot, *J. Phys. Chem. B* **102**, 5135 (1998).
- ⁹D. J. Coulman, J. Winterlin, R. J. Behm, and G. Ertl, *Phys. Rev. Lett.* **64**, 1761 (1990).
- ¹⁰A. F. Carley, P. R. Davies, R. V. Jones, K. R. Harikumar, G. U. Kulkarni, and M. W. Roberts, *Surf. Sci.* **447**, 39 (2000).
- ¹¹A. Bakke, H. Chen, and W. Jolly, *J. Electron Spectrosc. Relat. Phenom.* **20**, 333 (1980).
- ¹²C. R. Brundle and A. F. Carley, *Faraday Discuss. Chem. Soc.* **60**, 51 (1975).
- ¹³B. R. Strohmaier, D. E. Leyden, R. S. Field, and D. M. Hercules, *J. Catal.* **94**, 514 (1985).
- ¹⁴D. A. Outka and R. J. Madix, *Surf. Sci.* **137**, 242 (1984).
- ¹⁵G. Tibbetts, *J. Vac. Sci. Technol.* **15**, 497 (1978).
- ¹⁶D. Lichtman, J. H. Craig, V. Slater, and M. Drinkwine, *Appl. Surf. Sci.* **7**, 325 (1981).
- ¹⁷R. W. Joyner and M. W. Roberts, *Chem. Phys. Lett.* **60**, 459 (1979).
- ¹⁸J. H. Scofield, *J. Electron Spectrosc. Relat. Phenom.* **20**, 333 (1976).
- ¹⁹D. A. Outka, R. J. Madix, G. B. Fisher, and C. DiMaggio, *J. Phys. Chem. B* **90**, 4051 (1986).
- ²⁰F. Jensen, F. Besenbacher, E. Laegsgaard, and I. Stensgaard, *Phys. Rev. B* **41**, 10233 (1990).
- ²¹X.-C. Guo and R. J. Madix, *J. Phys. Chem. B* **105**, 3878 (2001).
- ²²X.-C. Guo and R. J. Madix, *Surf. Sci.* **367**, L95 (1996).
- ²³F. M. Leibsle, *Surf. Sci.* **311**, 45 (1994).
- ²⁴F. Besenbacher and I. Stensgaard, in *The Chemical Physics of Solid Surfaces*, Vol. 6, edited by D. A. King and D. P. Woodruff (Elsevier Science, New York, 1993), Chap. 15.
- ²⁵A. Atri, A. L. Johnson, and D. A. King, *Surf. Sci.* **254**, 65 (1991).